1972

Fatigue crack growth in welded beams, January 1972 73-37

Manfred A. Hirt

John W. Fisher

OFFICE
OF
RESEARCH

LEHIGH UNIVERSITY

FATIGUE CRACK GROWTH
IN WELDED BEAMS

by

M. A. Hirt
J. W. Fisher

January 1972

Fritz Engineering Laboratory Report No. 358.35

FATIGUE CRACK GROWTH IN WELDED BEAMS

by

M. A. Hirt

J. W. Fisher

Office of Naval Research
Contract N 00014-68-A-0514

January 1972

Fritz Engineering Laboratory Report No. 358.35

FATIGUE CRACK GROWTH IN WELDED BEAMS

By Manfred A. Hirt,[1] A.M.ASCE, and

John W. Fisher,[2] M.ASCE

INTRODUCTION

This paper evaluates the fatigue behavior of welded steel beams without attachments using the fracture mechanics concepts of stable crack growth. Earlier studies had indicated that various flaw conditions existed in welded beams. Both internal and external weld defects in the web-to-flange fillet weld were evaluated and discussed in detail in Refs. 4, 9 and 10. Internal pores caused by entrapped gas in the weldment are known to form a common defect. These gas pores and their effect on the fatigue behavior of welded beams are discussed in this paper.

A fracture mechanics model for cracks originating from the pores in the web-to-flange fillet weld is developed. Estimates of the stress-intensity factor are made that numerically describe the initial flaw condition. With the initial and final crack

---

[1] Structural Engr., Howard, Needles, Tammen & Bergendoff, Consulting Engineers, New York, N. Y.; formerly Research Assistant, Fritz Lab., Lehigh Univ., Bethlehem, Pa.

[2] Prof. of Civ. Engrg., Assoc. Director Fritz Engrg. Lab., Lehigh Univ., Bethlehem, Pa.

size known, a theoretical crack-growth equation was derived from the fatigue test data of the welded beams. The experimental data including an analysis of the test variables were presented in Refs. 4 and 9.

FATIGUE STRENGTH OF WELDED BEAMS WITH INTERNAL WELD DISCONTINUITIES

It was observed that cracks in the welded beams always originated from a discontinuity (flaw) in the web-flange fillet weld unless a severe notch existed at the flame-cut flange tip. More than 180 cracks were found in the plain-welded beams reported in Refs. 4 and 9. Seventy-five of these cracks were cut open for fractographic examination. It was found that about 80% of the cracks had originated from porosity caused by the entrapment of gas. In general, these cavities were completely inside the weld. The gas pores appeared on the fracture surface as rounded cavities with a smooth and shiny surface as illustrated in Fig. 1. A few pipe or blow holes extended to the surface of the weld.

All test data for beams failing from porosity in the longitudinal fillet weld are plotted by solid symbols in Fig. 2. The equation of the mean line resulting from a least squares fit to the test data is (see Fig. 2):

$$\text{Log } N = 10.3528 - 2.9844 \text{ Log } S_r \quad \ldots\ldots\ldots \quad (1)$$

Previous analysis (4,9) had indicated that stress range was the dominant variable and that grade of steel did not significantly affect the fatigue strength.

The open symbols in Fig. 2 indicate plain-welded beams that failed from defects other than porosity. This included beams failing from weld repairs, stop-start positions, other weld defects, and severe notches in the flame-cut flange-tips. Generally, these beams yielded shorter lives than beams failing from porosity.

When weld repairs were absent in the fillet weld of beams with stiffeners or attachments, failure occurred at these welded details since they were more critical than porosity. These beam data are also included as they revealed no visible crack growth in the longitudinal fillet weld at lower stress ranges. An indication of a run-out level is seen at the 18 ksi stress range level. Only three data points from plain-welded beams failing from porosity were observed at that stress range.

CRACK-GROWTH OBSERVATION ON A PLAIN-WELDED BEAM

A plain-welded beam was tested and closely observed in order to investigate crack formation and growth on the surfaces of the fillet weld, web and flange. Measurements of crack length and load were made so that crack-growth rates could be determined for the structural element.

Beam PWB-341 (4) was selected for this study since it had failed prematurely after 192,000 cycles of stress from a flange-tip crack. Replicate beams tested at the same stress range of 36 ksi indicated that a crack from a gas pore could be expected to become visible within an additional 200,000 cycles. The flange-tip crack was carefully repaired and testing was resumed under the same stress conditions. The fillet welds were searched for cracks using a regular hand magnifying glass while testing at 250 cycles per minute. A length of more than 42 inches of weld on both sides of the web in the constant moment region was observed. Testing was interrupted periodically so that the weld could be examined under static load. Suspicious locations were further examined with a 50-power microscope.

A hairline crack was detected on the weld surface shortly after an examination under static load. Testing was temporarily discontinued at that time after a total of 351,700 applied stress cycles. The apparent total crack-size visible on the weld surface was found to measure about 0.05-inch when the load was removed from the beam. This increased to 0.25-inch under maximum stress of 50 ksi in the extreme fibre.

A reference grid was placed on the inside surfaces and the extreme fibre of the flange as well as on both faces of the web. The grids were placed close to the cross section containing the hairline crack. It was possible to estimate the crack-tip to

within 1/5 of a grid line ($\pm$0.01-inch) using 50-power magnification. The hand magnifying glass permitted about 1/2 the grid distance to be estimated ($\pm$0.025-inch).

At intervals of about 18,000 cycles, testing was interrupted and the crack was measured under a statically applied maximum load. There was good agreement between the crack-length measurements under dynamic and static loading. Only the linear dimension of the crack on the fillet weld could be observed until the crack reached the extreme fibre. After about 435,000 cycles the crack was detected on the bottom surface of the flange. It was also observed that the crack had penetrated through the other fillet weld.

The increase in crack-size was very rapid after the crack had penetrated the bottom flange surface. The cross section of the flange fractured at 567,000 cycles as one crack-tip reached the flange-tip. A schematic of the advancement of the crack after it had penetrated the extreme fibre is shown in Fig. 3 and indicates a transition from a penny-shaped crack with a continuous crack front in the flange-web junction to a three-ended crack with two crack tips in the flange and one in the web.

Hence, two basic stages of growth were observed for cracks originating from pores in the longitudinal fillet weld of welded beams. The first stage of growth was in the flange-to-web junction from the initial crack-size up to the point where the

crack reached the extreme fibre of the flange. After penetration of the extreme flange-fibre, the crack changed its shape rapidly to become a three-ended crack.

A PENNY-SHAPED CRACK MODEL

Fractographic examination of small cracks that had originated from pores in the fillet weld showed that many were almost perfectly circular in shape. This circular shape was found at various stages of growth up to the point where the crack had reached the extreme fibre of the flange, as illustrated in Figs. 4, 5, and 6.

One of the smallest cracks was discovered when examining a crack in the fillet weld. A tiny crack about 0.07-inch in diameter had originated from a very small pore in the left weld as shown in Fig. 4. The extent of the circular crack is seen from the smooth crack surface surrounding the pore, as compared to the rough appearance caused by static tearing when the cross section was opened for inspection. The small crack on the left was completely inside the flange-to-web junction and could not be detected by inspection of the weld surface.

A small crack discovered by the magnetic particle inspection method is shown in Fig. 5. The crack had initiated from the elongated pore and grown to the surface of the fillet weld. Almost no deviation from a circular shape is visible.

This crack is about 0.26-inch diameter and could not be detected on the weld surface with the aid of a magnifying glass even under favorable circumstances and under sustained loading.

A crack which has nearly penetrated the extreme fibre of the tension flange is shown in Fig. 6. Again, no significant disturbance of the circular shape is apparent at either side of the web or at the front approaching the surface of the flange. This crack, although quite sizeable, is not easily detected on a structural element under applied loading. The linear dimension of the crack visible on the surface of the flange-to-web junction is somewhat less than an inch.

This phenomenon of a circular crack-shape, seemingly not influenced by the free surfaces, is believed to be a consequence of the compatibility condition of the basically elastic cross section. Based on this photographic evidence, a circular disc-like crack was assumed to model the actual crack during growth inside the flange-web connection as was illustrated in Fig. 3.

EVALUATION OF FATIGUE BEHAVIOR USING FRACTURE MECHANICS CONCEPTS

The fatigue test data and fractographic observations of small fatigue cracks suggested that fracture mechanics of stable crack-growth might be useful in evaluating the observed

behavior of the test beams. The stress intensity factor K introduced by Irwin (11) describes in convenient form the influence of the stresses, applied sufficiently away from the crack tip, and the crack size a. The relative size is usually expressed in terms of a correction function, f(a), where the linear dimensions of the plate, or the distance to a free edge or surface, are introduced.

$$K = \sigma \sqrt{\pi a}\, f(a) \qquad (\text{ksi}\sqrt{\text{in.}}) \quad . \quad . \quad . \quad . \quad . \quad . \quad . \quad . \quad . \quad (2)$$

Paris (15) has suggested the following relationship between the rate of crack propagation and the change in the stress-intensity factor:

$$\frac{da}{dN} = C\,\Delta K^{n} \quad . \quad . \quad . \quad . \quad . \quad . \quad . \quad . \quad . \quad . \quad . \quad . \quad . \quad . \quad . \quad . \quad . \quad . \quad . \quad (3)$$

This model expresses crack growth per cycle, $\frac{da}{dN}$, in terms of the variation of the stress intensity factor, ΔK, and two material constants, C and n.

For the case of a crack with constant correction factor, f(a), and subjected to constant amplitude stress, integration of Eq. 3 yields

$$N_{ij} = \frac{1}{C} \cdot \frac{1}{\alpha\, f^{n}(a)\, \pi^{n/2}\, \Delta\sigma^{n}} \left(a_i^{-\alpha} - a_j^{-\alpha}\right) \quad . \quad . \quad . \quad . \quad (4)$$

where $\alpha = \frac{n}{2} - 1$. For specimens with equal initial crack-size a_i, final crack-size a_j, and identical boundary conditions, a

theoretical value for the prediction of the life interval N_{ij} can be expressed in terms of a new constant C' times the applied stress range $\Delta\sigma$ as

$$N_{ij} = C' \Delta\sigma^{-n} \quad \ldots\ldots\ldots\ldots\ldots\ldots \quad (5)$$

where

$$C' = \frac{1}{C} \cdot \frac{1}{\alpha f^{n}(a) \pi^{n/2}} (a_i^{-\alpha} - a_j^{-\alpha}) \quad \ldots\ldots \quad (6)$$

The log-log transformation of Eq. 6 yields a straight line of the form

$$\text{Log } N_{ij} = \text{Log } C' - n \text{ Log } (\Delta\sigma) \quad \ldots\ldots\ldots \quad (7)$$

APPLICATION TO THE PLAIN-WELDED BEAM

In order to apply the outlined concepts of fracture mechanics a reasonable characterization of the flaws was needed. A large number of cracks that originated from porosity in the fillet weld were examined closely to establish the initial flaw condition. The flaws were photographed and enlarged at least three times as was illustrated in Fig. 1. The dimensions of the defects were measured under 10-power magnification.

Cracks were examined in beams fabricated from three different grades of steel. The estimated K-values corresponding to the measured flaw dimensions are summarized in Fig. 7 in a

log-log presentation of $\Delta K/\Delta\sigma$ versus the controlling crack-size a. The estimate for the defect that corresponds to the largest observed crack from each beam is indicated by a solid symbol. The estimated K-values were obtained using a circumscribed ellipse for flaws similar to the shapes illustrated in Fig. 1(a) and Fig. 6. For flaws comparable to those shown in Fig. 1(b) and Fig. 5, the K-estimate at the narrow transition from the circular void to the elongated pore was generally used.

It was previously concluded from fractographic inspection of very small fatigue cracks (Figs. 4 and 5) that a penny-shaped crack-model described the shape of these cracks during crack growth. However, the estimated K-values for the initial flaws shown in Fig. 7 represent a collection of elliptical shapes with various a/b-ratios. Hence, each individual defect was transformed into a penny-shaped crack with an "equivalent crack-radius a_e" corresponding to the estimated $\Delta K/\Delta\sigma$-value. The sample of the resulting equivalent crack-radii is indicated at the bottom of Fig. 7. An average equivalent crack-radius a_e = 0.04-inch was selected to represent the sample of measured pores. The initial crack-radius a_i was assumed equal to this average value.

Derivation of Crack-Growth Constants.- The coefficients of the crack-growth equation can now be established from the equivalence of the coefficients in Eqs. 1 and 7. Equation 7 is the theoretical prediction of the fatigue life using fracture

mechanics concepts, and Eq. 1 expresses the statistical mean line of the relevant fatigue test data shown by solid dots in Fig. 2. The following assumptions were made to assist with the evaluation of the crack-growth constants, C and n:

(1) The crack was assumed to be described by a disc-like penny-shaped crack with a constant correction factor f(a) over the interval of integration. The correction factor f(a) for a penny-shaped crack is $2/\pi$.

(2) The estimates of the initial and final crack-radii a_i and a_j were available from visual observations. The average initial crack-radius a_i was assumed to equal the estimate of the equivalent crack-radius a_e = 0.04-inch from Fig. 7 representing the sample of measured pores.

The final crack-radius a_j was assumed to be reached when the crack had penetrated the extreme fibre of the flange. The life remaining after this occurred was at most 10% of the total fatigue life of the beam as was illustrated by the measurements given in Fig. 3. The final crack-radius was assumed to be equal to the nominal flange thickness. Experimental observations indicated this to be reasonable.

(3) It was assumed that all three grades of steel could be represented by the same crack-growth equation.

This assumption was based on results of tests on the welded beams. It was shown in Ref. 4 that grade of steel did not significantly influence the fatigue life of the beams.

Equating the values of the coefficients for the mean regression curve (Eq. 1) to the coefficients n and C', (Eq. 7) and substituting the crack-radii a_i and a_j, and the correction factor f(a) into Eq. 6 yields growth constants $n \cong 3$ and $C = 2.05 \times 10^{-10}$. Substitution of these constants into Eq. 3 numerically describes the crack-growth rate in terms of ΔK:

$$\frac{da}{dN} = 2.05 \times 10^{-10} \Delta K^3 \quad \ldots\ldots\ldots\ldots\ldots\ldots \quad (8)*$$

COMPARISON OF DERIVED CRACK-GROWTH EQUATION WITH MEASURED CRACK-GROWTH RATES

Equation 8 is plotted in Fig. 8 and compared with the various stages of crack growth in the test beam illustrated in Fig. 3. The straight line estimate for crack growth as a penny-shaped crack from crack initiation until penetration of the extreme fibre is indicated. Also shown are the data points for the observed crack-growth rates on the inside and outside surfaces of

---

* The dimensions used for crack-growth rates, $\frac{da}{dN}$, were inch/cycle, and the stress-intensity factor range, ΔK, was ksi $\sqrt{\text{in.}}$

the flange for growth as a three-ended crack.

It is apparent from Fig. 8 and the schematic shown in Fig. 3 that most of the life is spent growing the crack from its initial equivalent flaw radius, a_e = 0.04-inch, to its penetration of the extreme fibre of the flange, a_f = 0.375-inch. The corresponding range of ΔK for the test beam was between 8 ksi $\sqrt{in.}$ and 25 ksi $\sqrt{in.}$ under a constant amplitude stress range of 36 ksi while 435,000 cycles elapsed. The transition from a penny-shaped crack to a three-ended crack only required about 16,000 cycles. An additional 10,000 cycles were required to grow the crack large enough to cause net-section yielding. Final failure terminated testing at 467,000 cycles.

It is also apparent from Fig. 8 that most of the life was spent while growth occurred in a region of small ΔK. This is particularly true for lower applied stress ranges as illustrated in Fig. 9. The ΔK-regions applicable to growth as a penny-shaped crack are indicated for the test beams subjected to the stress ranges used in this study. Crack initiation took place at ΔK-values below 10 ksi $\sqrt{in.}$ in all test beams. Most of the life was spent at growth rates smaller than 10^{-6} inch/cycles.

The derived crack-growth relationship given by Eq. 8 is also compared with data from crack-growth specimens in Fig. 9. It was necessary to extrapolate the curve into the higher growth rate region since very little data was available at the lower growth

rate levels. The extrapolated curve falls within the scatterband reported by Crooker and Lange (3). This scatterband contains data from tests on carbon and low-alloy steels with yield strengths between 34 ksi and 127 ksi. This is comparable to the yield strengths of the steel beams. A conservative upper bound for growth rates on ferrite-pearlite steels was proposed by Barson (1) as

$$\frac{da}{dN} = 3.6 \times 10^{-10} \Delta K^3 \quad \ldots\ldots\ldots\ldots\ldots\ldots \quad (9)$$

This relationship is parallel to Eq. 8.

Since much of the growth in the plain-welded beams took place in the weld metal and heat affected zone, a comparison of the theoretical curve with Maddox's data (13) is relevant. An approximate envelope for Maddox's data on four different weld metals is shown. Three had about equal yield strength (67 ksi), the fourth had a higher yield point equal to 90 ksi. Also included in the scatterband are test data for a simulated heat affected zone in mild steel material with the same yield strength. The correlation with these crack-growth data is good.

It is apparent from Fig. 9 that the Crooker-Lange scatterband does not cover the critical region of interest for plain-welded beams. Most studies of crack-growth rates have been limited to larger ΔK-values and higher crack-growth rates because of the difficulties encountered in the slow growth region.

However, the theoretical curve (Eq. 8) extrapolated into the higher ΔK-regions shows the same general trend reported by others on basic crack-growth specimens (Fig. 9). The theoretical curve is just above the crack-growth data and underestimates their growth rate. This is surprising since the penny-shaped crack assumes the best condition for the crack in the welded beams and neglects the influence of free surfaces. This underestimate in growth rate may be due to crack initiation or an overestimate of the stress intensity.

The exponent, n, of the predicted crack-growth equation was about equal to 3.00 (Eq. 8). It represents the slope of the fatigue test data on plain-welded beams fabricated from three grades of steel. Crooker and Lange (3) observed from a review of the literature that the value of the slope n fell between 2 and 4 for a large range of steels. Gurney (6) reported the slope of the curve to be a linear function of yield stress of the material. A general trend observed in crack-growth studies is for the value of the exponent, n, to decrease with increasing yield strength of the material. This trend was not as pronounced in the welded-beam study. The exponent n did not appear to vary greatly from 3.

Careful evaluation of the coefficients n and C is needed for a wider range of rates of growth. Most of the data generally used to fit the straight line approximation only extend over a small range of ΔK. In other cases, data points at the

extremes cause rotation of the line. Substantial over- or under-estimates of the fatigue life of a structural component might result if these relationships are used to extrapolate beyond the range of the test data.

Very Slow Growth.- Johnson and Paris (12) have suggested that a threshold exists for crack growth. A recent investigation by Paris (16) on ASTM 9310 steel has provided more information on this phenomenon of very slow growth. The test specimens were pre-cracked and growth data for small ΔK-values obtained. The value of ΔK was then reduced stepwise and observations made on the relative crack-growth rates until a "threshold value" was reached. When ΔK was increased in steps, the rate of growth was comparable to the rates obtained by previous overloading. An approximate mean line fit to Paris' data is compared in Fig. 10 with Eq. 8. A drastically reduced growth rate for $\Delta K \cong 5.2$ ksi $\sqrt{\text{in.}}$ is observed. Similar deviations from the straight line approximation are found for large ΔK-values indicating an increased growth-rate. These observations will not be discussed in this paper as they apply mainly to low cycle fatigue problems.

Harrison (7) has reviewed the literature for run-out data on a variety of specimens. He concluded that "for all materials with the exception of pure aluminum, cracks will not propagate if $\frac{\Delta K}{E} < 1 \times 10^{-4} \sqrt{\text{in.}}$" He also found for a number of materials

that the limit for non-propagating cracks fell between $\frac{\Delta K}{E} = 1.5 \times 10^{-4} \sqrt{\text{in.}}$ and $1.8 \times 10^{-4} \sqrt{\text{in.}}$ Harrison's levels for four types of steel are also shown in Fig. 10, and are between 3.3 ksi $\sqrt{\text{in.}}$ for mild steel and 5.3 ksi $\sqrt{\text{in.}}$ for austenitic steel.

Influence of Defect-Size on Fatigue Life.- The life interval between two crack-sizes a_i and a_j can be determined from Eq. 4. For a given final crack-size, the computed number of cycles can be expressed as a function of the initial crack-size for a given stress range, as shown by the curved lines in Fig. 11. The final crack-radius for the penny-shaped crack-model was assumed equal to the flange-thickness of the welded test beams. This becomes less important for larger differences between initial crack-radius a_i and final radius a_j.

Alternately, the observed fatigue life of a tested beam can be used with the appropriate stress-range line to estimate the equivalent initial pore-radius that caused failure. The fatigue data of beams failing from porosity were shown in Fig. 2 and are replotted in this manner in Fig. 11. The resulting scatter of the equivalent pore-radii derived from the fatigue test data is shown on the right ordinate.

The equivalent pore-radii determined independently from measured flaws are shown on the left ordinate of Fig. 11. The scatter of the porosity as derived from the fatigue test data (right ordinate) is seen to be similar to the scatter from the

measured equivalent pore-sizes (left ordinate).

Hence, if no variation is assumed in the crack-growth characteristics, this comparison suggests that the scatter in the fatigue test data is caused by the variation in the initial crack-size. This is essentially the same conclusion reached by Harrison (8) for the analysis of test results from butt welds with lack of penetration defects. He concluded that the width of the scatterband probably resulted from variations in initial radii at the defect-tips.

Predictions of Fatigue Life using Different Crack-Models.- Additional crack-models were used to assess their influence on the prediction of the fatigue life. Figure 12 summarizes the results for the various models used. Six A441 steel beams were selected for the comparison. The actually observed fatigue lives of these six beams are shown by solid dots together with the mean and the 95% confidence interval for all test beams failing from porosity.

The defects that caused crack growth and failure of the six beams were examined. They were assumed to be characterized by a circumscribed ellipse with half-axes a and b. The following models were used to estimate the fatigue life of each individual beam using the known dimensions of the circumscribed ellipse, and employing crack-growth Eq. 8.

Model (a) The open circles in Fig. 12 correspond to the life estimates for the penny-shaped crack with equivalent crack-radius. The equivalent crack-radius was computed from the equivalence of the K-value with the circumscribed elliptical crack.

Model (b) Penny-shaped cracks were assumed to inscribe and circumscribe the ellipse. The shortest life estimates resulted from the circumscribed crack and the longest from the inscribed crack. These two estimates constitute "upper and lower bounds" and are indicated by the horizontal T-symbols in Fig. 12.

Model (c) Additional life estimates were made based on the elliptical crack-model. Growth was assumed in the direction of the minor axis 2a with constant major axis 2b until the size of the circumscribed crack was reached. The computation of the increment of life from an elliptical to a circular crack was done using an available computer program (5). Numerical integration was employed because of the variable correction factor f(a). This increment of life was added to the estimate for the circumscribed penny-shaped crack. The total life estimate is indicated by triangles in Fig. 12.

The comparison between the estimates for each individual beam provided by the different models and the observed fatigue life permitted the following observations to be made:

(1) The life estimates employing the equivalent penny-

shaped crack-radius [model (a)] resulted in slightly shorter lives than the estimates that assumed the elliptical crack first to grow to a circular shape [model (c)].

(2) Both of these estimates were bounded by the estimates provided by the inscribed and circumscribed initial cracks [model (b)].

(3) The observed fatigue data were also contained within the bounds from the estimates of the circumscribed and inscribed circles in all but one case.

(4) Long flaws with small a/b-ratios [as illustrated in Fig. 1(b)] provided the greatest deviation between the computed "lower and upper bounds."

(5) All three defects of the type shown in Fig. 1(a) had their life underestimated when the equivalent initial crack-radius was used [model (a)]. The estimate improved for the elliptical model (c).

(6) Most of the estimates from models (a) and (c) fell within the two limits of dispersion representing the 95% confidence interval of all the beam test data. The selection of a penny-shaped crack model did not introduce more scatter than was experimentally observed from fatigue test data.

Prediction of Fatigue Life using Measured Crack-growth Rates.- Maddox (14) and Harrison (8) have demonstrated that good predictions of the fatigue life can be obtained from crack-growth data. Barsom's (1) conservative estimate of crack-growth rate, Eq. 9, for ferrite-pearlite steels was used to predict the fatigue life of the beams failing from porosity. The result is shown in Fig. 13 together with the applicable welded beam test data and the respective mean line and the 95% confidence interval.

Also shown in Fig. 13 is the prediction based on Paris' data (16), indicating a threshold level for run-out at about 23 ksi stress range. This prediction was obtained using the straight line segments shown in Fig. 10 which approximate the data from the study on very slow growth. The threshold values by Harrison (7) shown in Fig. 10 were also used to estimate run-out. Run-out tests are predicted to occur at levels as high as 20 ksi stress range for low-alloy steel, as shown by the horizontal lines in Fig. 13.

The predictions based on the crack-growth data underestimate the mean fatigue life of the test beams at the higher stress range levels. This was expected from the comparison of the crack-growth data. Since any assumption other than a penny-shaped crack-model for the welded beams would further reduce the life prediction based on crack-growth data, a crack-initiation period may be responsible for the slight underestimate. Other factors

that could be responsible for the underestimate in life are an overestimate of the initial crack-size, an overestimate of the stress intensity, or a slower growth rate under plane-strain conditions (7).

The scatter in the test data shown in Fig. 13 was previously related to the variation in shape, size and severity of the porosity. Other factors contribute to the variation in test data. Beams with seemingly equal defects still experience scatter in the fatigue strength because of variation in the crack tip radius, crack-growth rates, and other uncontrolled variables.

SUMMARY AND CONCLUSIONS

The main findings of this study are summarized hereafter. They are based on a detailed examination of the test data, fracture surfaces, initial flaw conditions provided by the experimental work, and on the theoretical studies of stable crack growth.

(1) The characterization of the initial flaw condition revealed porosity to be the most common defect in plain-welded beams. The distribution of the size and location of the pores in the longitudinal fillet weld was random. The welded beam fatigue data fell within a narrow scatterband when plotted as the logarithmic transformation of stress range and cycles to failure.

(2) Fracture mechanics concepts provided a rational way to analyze and characterize the behavior of welded and rolled beams. These concepts were applied to describe numerically the initial flaw conditions in welded beams, and to derive a crack-growth rate vs. range of stress-intensity relationship from welded-beam fatigue data.

(3) A penny-shaped crack was found to model crack growth from porosity in welded beams. An equivalent crack with a 0.04-inch radius described the average pores observed in the welded beams.

(4) The derived crack-growth equation exhibited the same trend as measured data from crack-growth specimens. It provided a lower estimate of the growth rate. Among other factors, this difference was attributed to crack initiation, a possible overestimate of the stress intensity, and slower growth in the plane-strain condition for the welded beams.

(5) Available crack-growth data were shown to only cover a small region of growth rates. Extrapolation into regions outside the data could be misleading, particularly when used for fatigue life estimates.

(6) Very little information is available for growth rates below 10^{-6} inch/cycles. This was found to

be the region most critical for the fatigue behavior of welded and rolled beams. More than 75% of the life was spent in this region growing a crack from its initial size to a visible crack.

(7) It was shown that the initial crack-size was the controlling factor for the fatigue life of welded beams. An increase in flange-thickness and larger weld-sizes should hence not permit an increase in allowable defect-size.

(8) The scatter of the fatigue data was found to be related in part to the variation in the initial flaw-condition and in part to the variation in fatigue crack-growth rates or other uncontrolled variables.

ACKNOWLEDGEMENTS

This paper is based in part on the experimental and theoretical investigations made during the course of a research program on the effect of weldments on the fatigue strength of steel beams. Partial support was also provided by the Office of Naval Research, Department of Defense, under Contract N00014-68-A-514; NR064-509. The experimental research was performed under National Highway Research Program Project 12-7 at Fritz Engineering Laboratory, Department of Civil Engineering, Lehigh University, Bethlehem, Pa.

The authors wish to express their appreciation for the helpful suggestions made by Profs. G. R. Irwin, A. W. Pense, and R. W. Hertzberg on the fracture mechanics and metallurgical aspects of this work. Special thanks are due Karl H. Frank and Ben T. Yen for the cooperation and challenging discussions during the progress of this study.

APPENDIX I.-REFERENCES

1. Barsom, J. M., "Fatigue-crack Propagation in Steels of Various Yield Strengths," U. S. Steel Corp., Applied Research Laboratory, Monroeville, Pa., 1971.

2. Clark, W. G. Jr., and Trout, H. E. Jr., "Influence of Temperature and Section Size on Fatigue Crack Growth Behavior in Ni-Mo-V Alloy Steel," Engineering Fracture Mechanics, Vol. 2, No. 2, November, 1970, pp. 107-123.

3. Crooker, T. W., and Lange, E. A., "How Yield Strength and Fracture Toughness Considerations Can Influence Fatigue Design Procedures for Structural Steels," Welding Research Supplement, Vol. 49, No. 10, October, 1970, pp. 488-496.

4. Fisher, J. W., Frank, K. H., Hirt, M. A., and McNamee, B. M., "Effect of Weldments on the Fatigue Strength of Steel Beams," NCHRP Report No. 102, Highway Research Board, National Academy of Sciences - National Research Council, Washington, D. C., 1970.

5. Frank, K. H., and Fisher, J. W., "Analysis of Error in Determining Fatigue Crack Growth Rates," Report No. 358.10, Lehigh University, Fritz Engineering Laboratory, March, 1971.

6. Gurney, T. R., "An Investigation of the Rate of Propagation of Fatigue Cracks in a Range of Steels, Members' Report No. E18/12/68, The Welding Institute, December, 1968.

7. Harrison, J. D., "An Analysis of Data on Non-Propagating Fatigue Cracks on a Fracture Mechanics Basis," Metal Construction and British Welding Journal, Vol. 2, No. 3, March, 1970, pp. 93-98.

8. Harrison, J. D., "The Analysis of Fatigue Test Results for Butt Welds with Lack of Penetration Defects Using a Fracture Mechanics Approach," Welding in the World, Vol. 8, No. 3, 1970, pp. 168-181.

9. Hirt, M. A., Yen, B. T., and Fisher, J. W., "Fatigue Strength of Rolled and Welded Steel Beams," Journal of the Structural Division, ASCE, Vol. 97, No. ST7, July, 1971, pp. 1897-1911.

10. Hirt, M. A., "Fatigue Behavior of Rolled and Welded Beams," Ph.D. Dissertation, Lehigh University, Department of Civil Engineering, October, 1971.

11. Irwin, G. R., "Analysis of Stresses and Strains near the End of a Crack Traversing a Plate," Transactions, ASME, Series E, Vol. 24, No. 3, September, 1957, pp. 361-364.

12. Johnson, H. H., and Paris, P. C., "Sub-Critical Flaw Growth," Engineering Fracture Mechanics, Vol. 1, No. 1, June, 1968, pp. 3-45.

13. Maddox, S. J., "Fatigue Crack Propagation in Weld Metal and Heat Affected Zone Material," Members' Report No. E/29/69, The Welding Institute, December, 1969.

14. Maddox, S. J., "The Propagation of Part-through-Thickness Fatigue Cracks Analysed by Means of Fracture Mechanics," Members' Report No. E/30/69, The Welding Institute, December, 1969.

15. Paris, P. C., "The Fracture Mechanics Approach to Fatigue," Fatigue - An Interdisciplinary Approach, Proceedings, Tenth Sagamore Army Materials Research Conference, Syracuse University Press, Syracuse, N. Y., 1964, p. 107.

16. Paris, P. C., "Testing for Very Slow Growth of Fatigue Cracks," Closed Loop, MTS Systems Corp., Vol. 2, No. 5, 1970, pp. 11-14.

APPENDIX II.-NOTATION

C	a material related constant in crack-growth equation
K	elastic stress-intensity factor for a crack; (ksi $\sqrt{}$in.)
N	number of applied stress cycles

N_{ij}	number of cycles required for a crack to grow from size a_i to size a_j
S	nominal applied stress in the extreme fibre of the tension flange
S_r	stress range
a	crack size; crack-radius for penny-shaped crack, half crack-width for tunnel crack or through-the-thickness crack, crack-depth for surface crack, crack-radius for corner crack, minor half-axis for elliptical crack
a_e	equivalent radius of a penny-shaped crack that provides the same K-factor estimated for the arbitrarily shaped crack
a_f	final crack-size
a_i	initial crack-size (for integration interval)
a_j	final crack-size (for integration interval)
b	major half-axis for an elliptical crack
f(a)	nondimensional geometry correction factor for stress-intensity factor K
n	exponent of crack-growth equation; slope of equation in log-log transformation
α	$\frac{n}{2} - 1$
ΔK	stress-intensity-factor range
$\Delta\sigma$	stress range relevant for the determination of the stress-intensity-factor range
σ	stress applied sufficiently away from the crack-tip

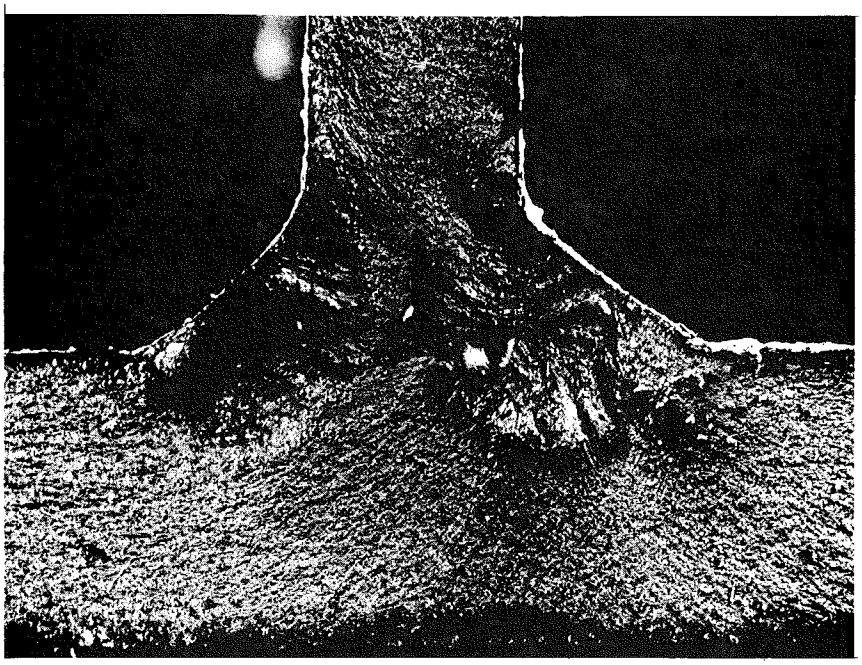

(a) Typical gas pore (x4)

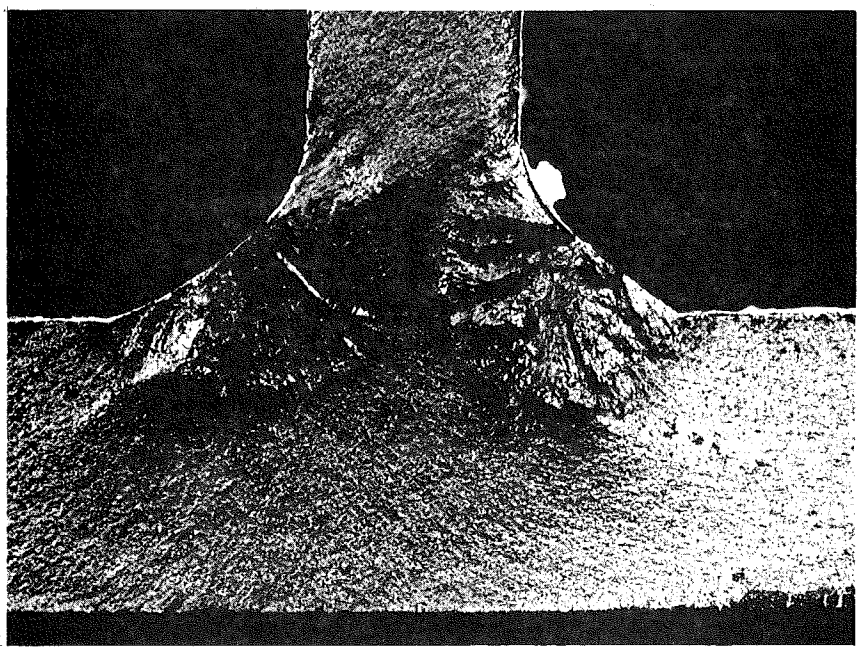

(b) Pore elongated and perpendicular to the weld surface (x4)

Fig. 1 Examples of porosity from the root of the longitudinal fillet-weld

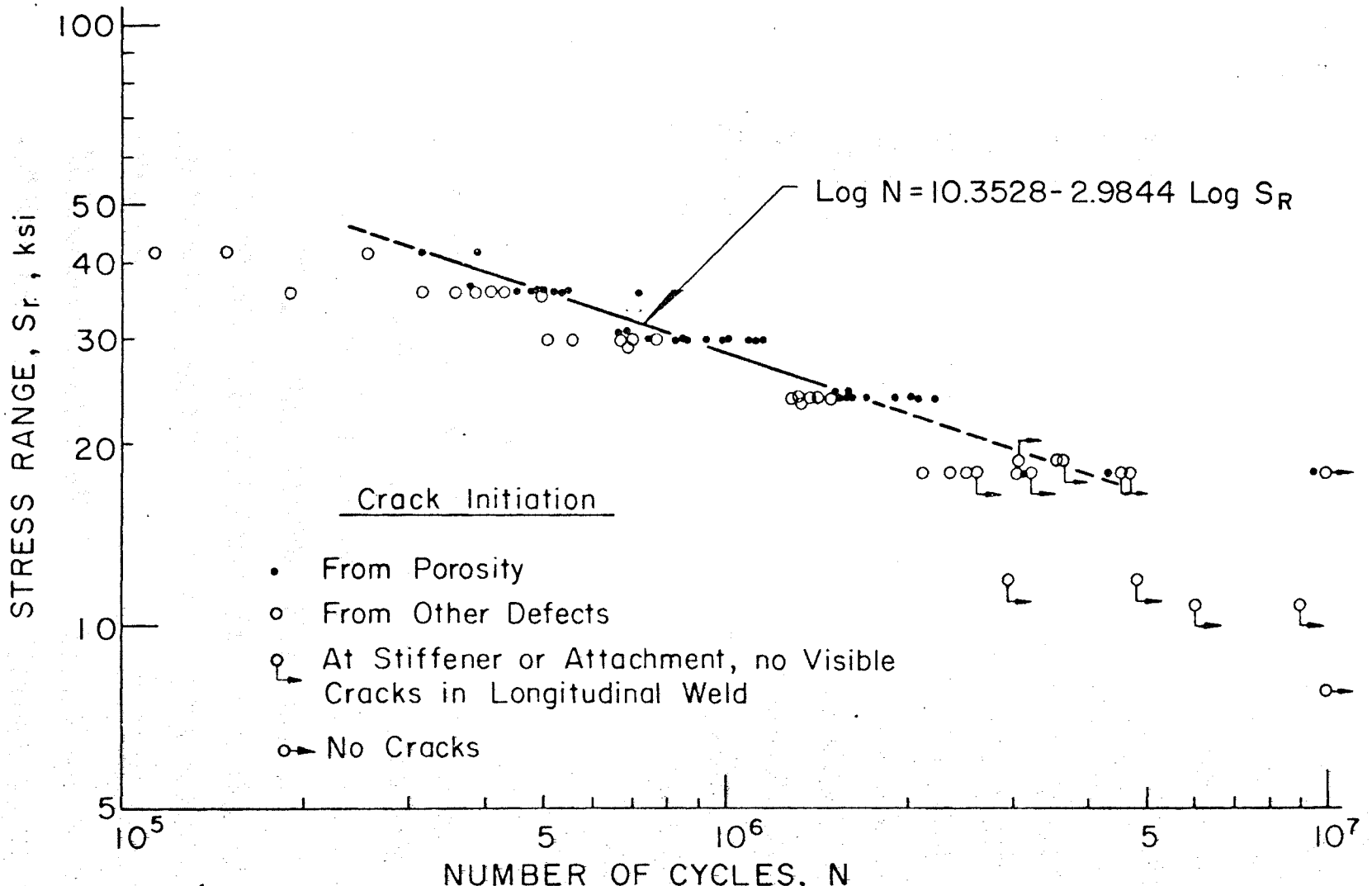

Fig. 2 Comparison of all welded beams failing from porosity in the fillet weld with beams failing from other defects

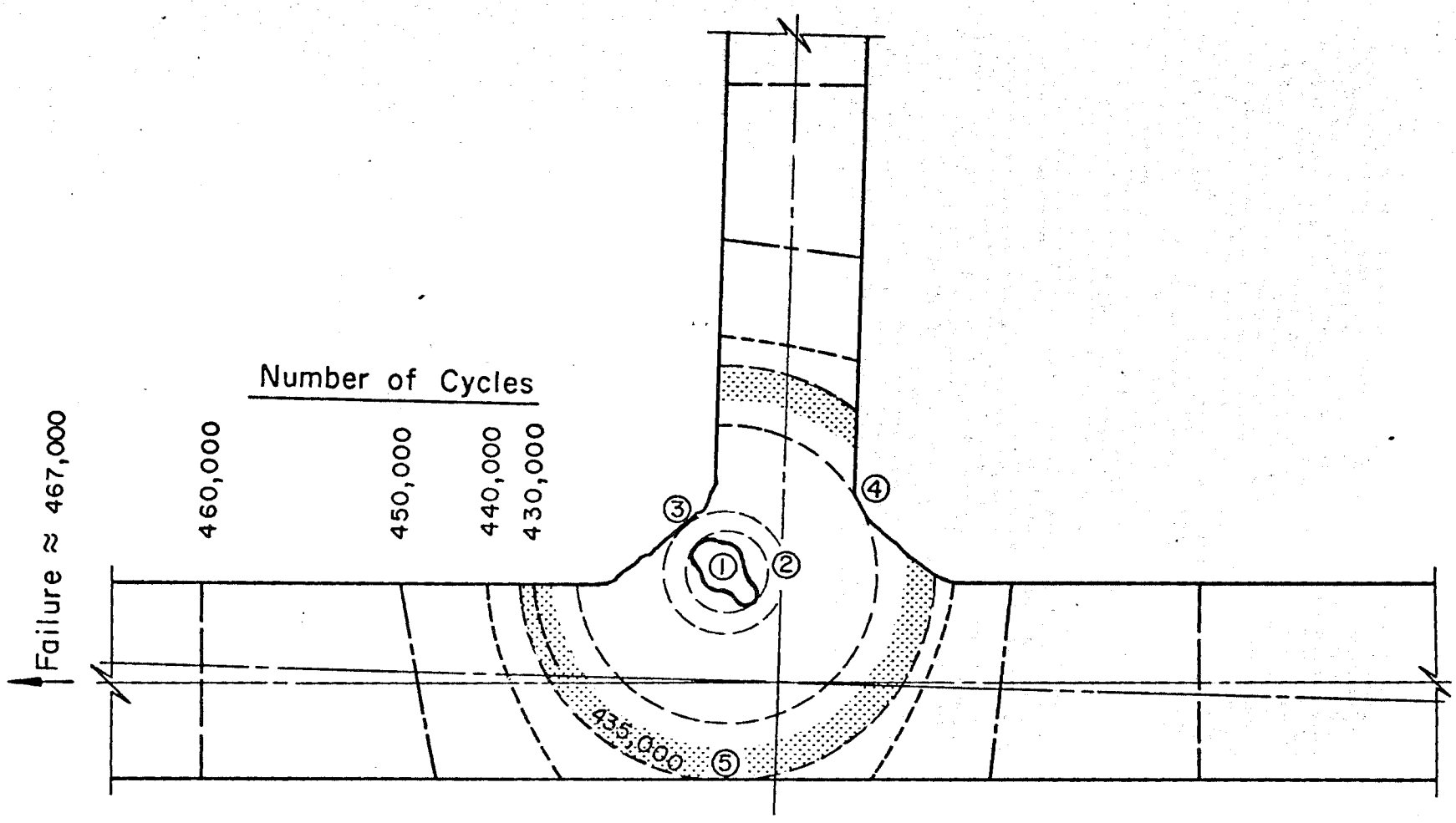

Fig. 3 Schematic of the stages of crack growth from a pore in the fillet weld

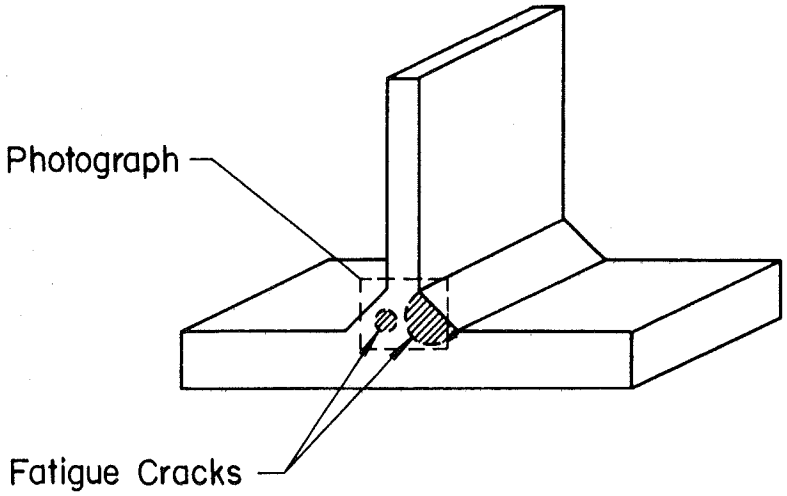

Fig. 4 Two small fatigue cracks that initiated from pores in the longitudinal fillet-weld and grew perpendicular to the axis of the weld (~x8.5)

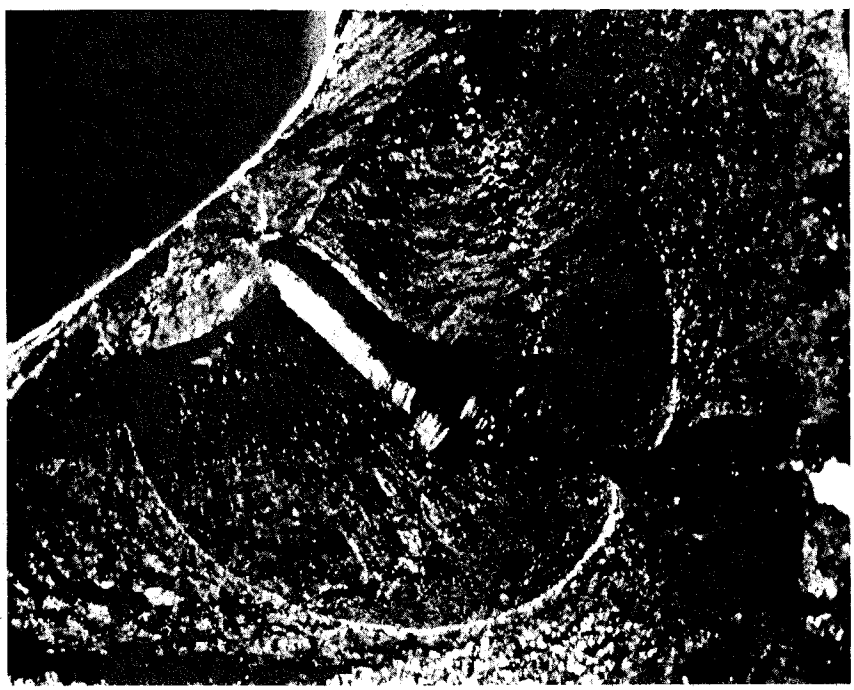

Fig. 5 Small crack with penetration to the fillet-weld surface (~x11)

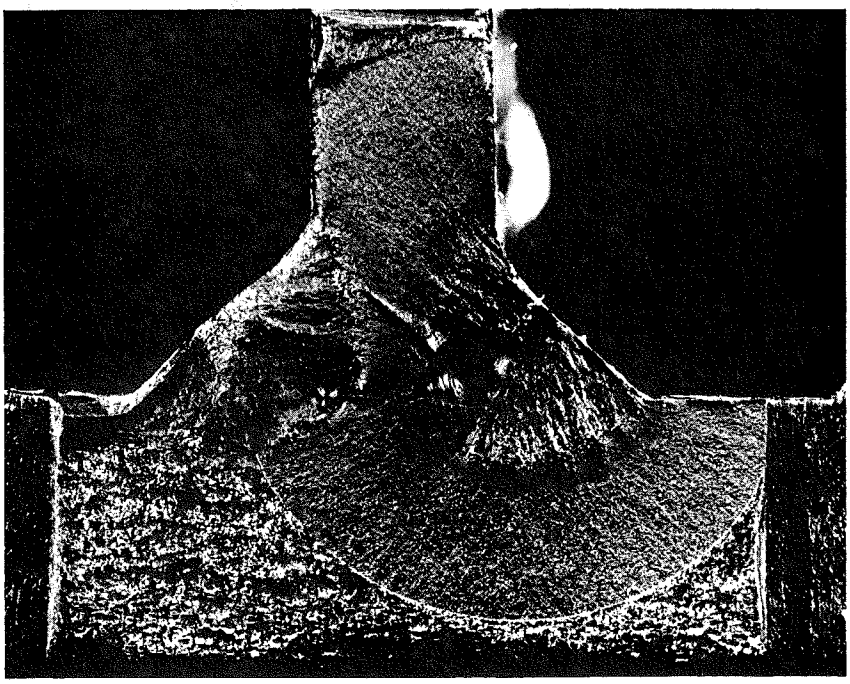

Fig. 6 Crack in flange-to-web junction approaching the extreme fibre of the tension flange (x3.6)

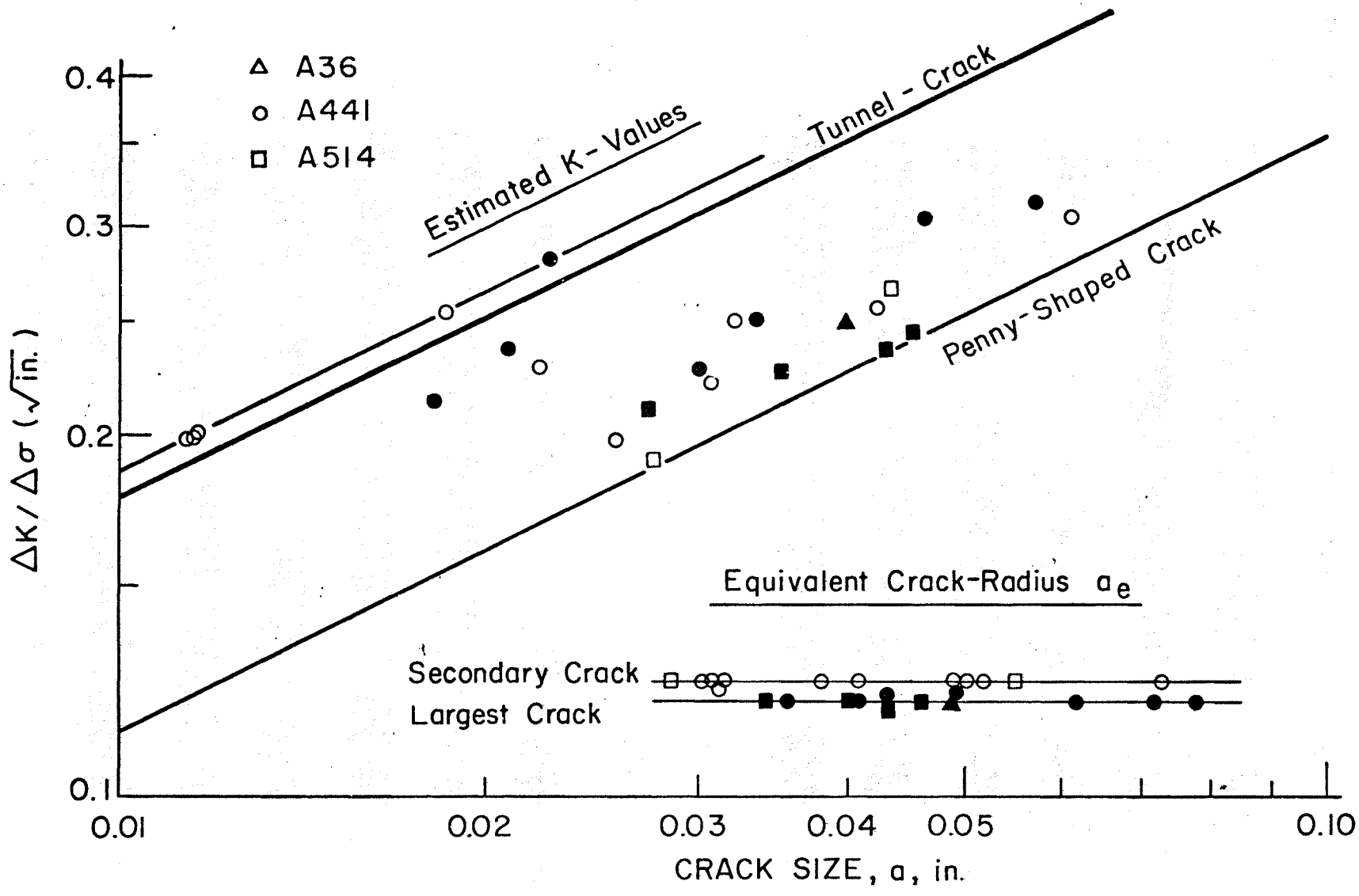

Fig. 7 Distribution of estimated K-values and equivalent crack-radii

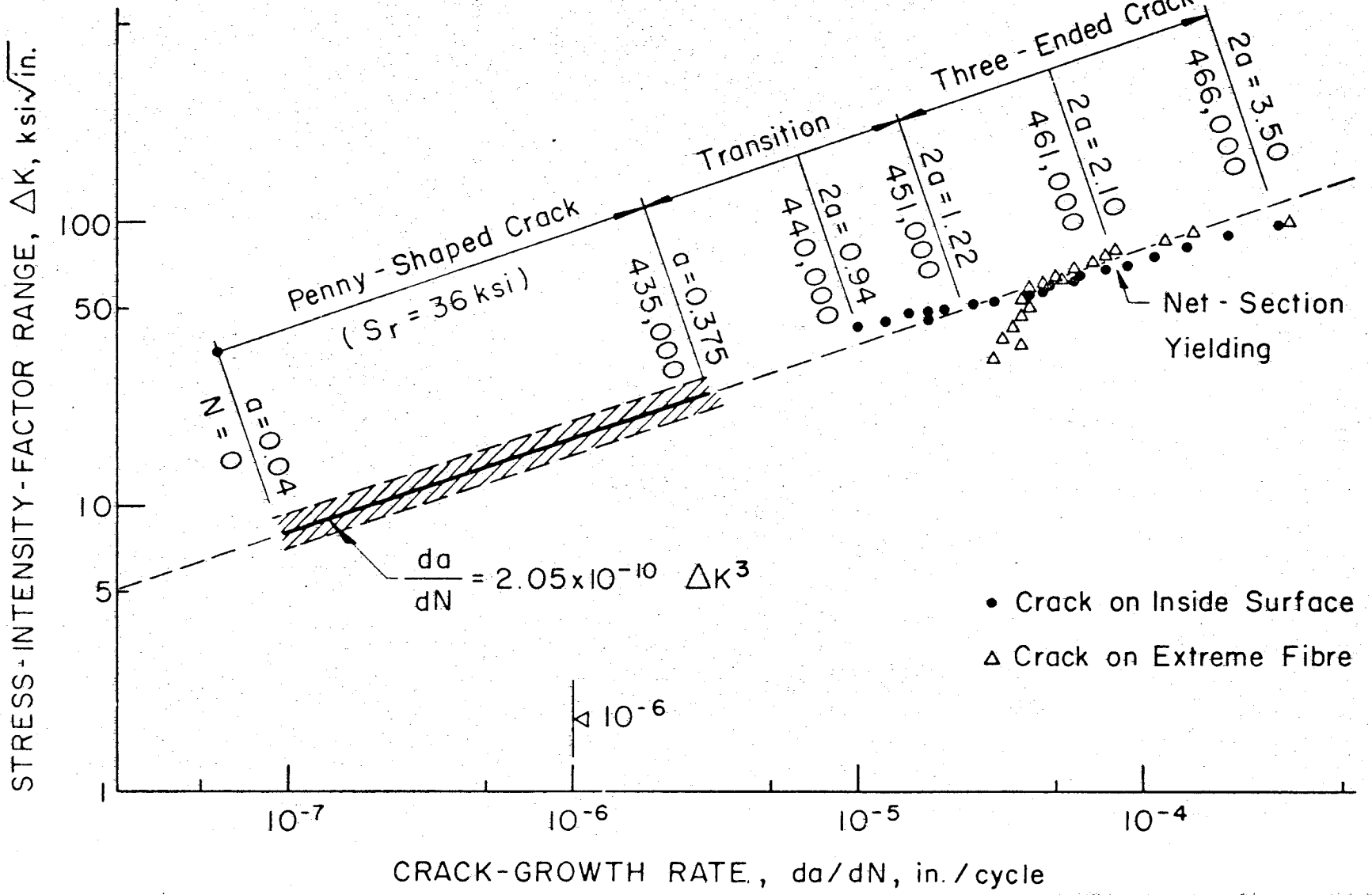

Fig. 8 Various stages of crack growth and corresponding growth rates for a crack in a plain-welded beam starting from a pore in the fillet weld

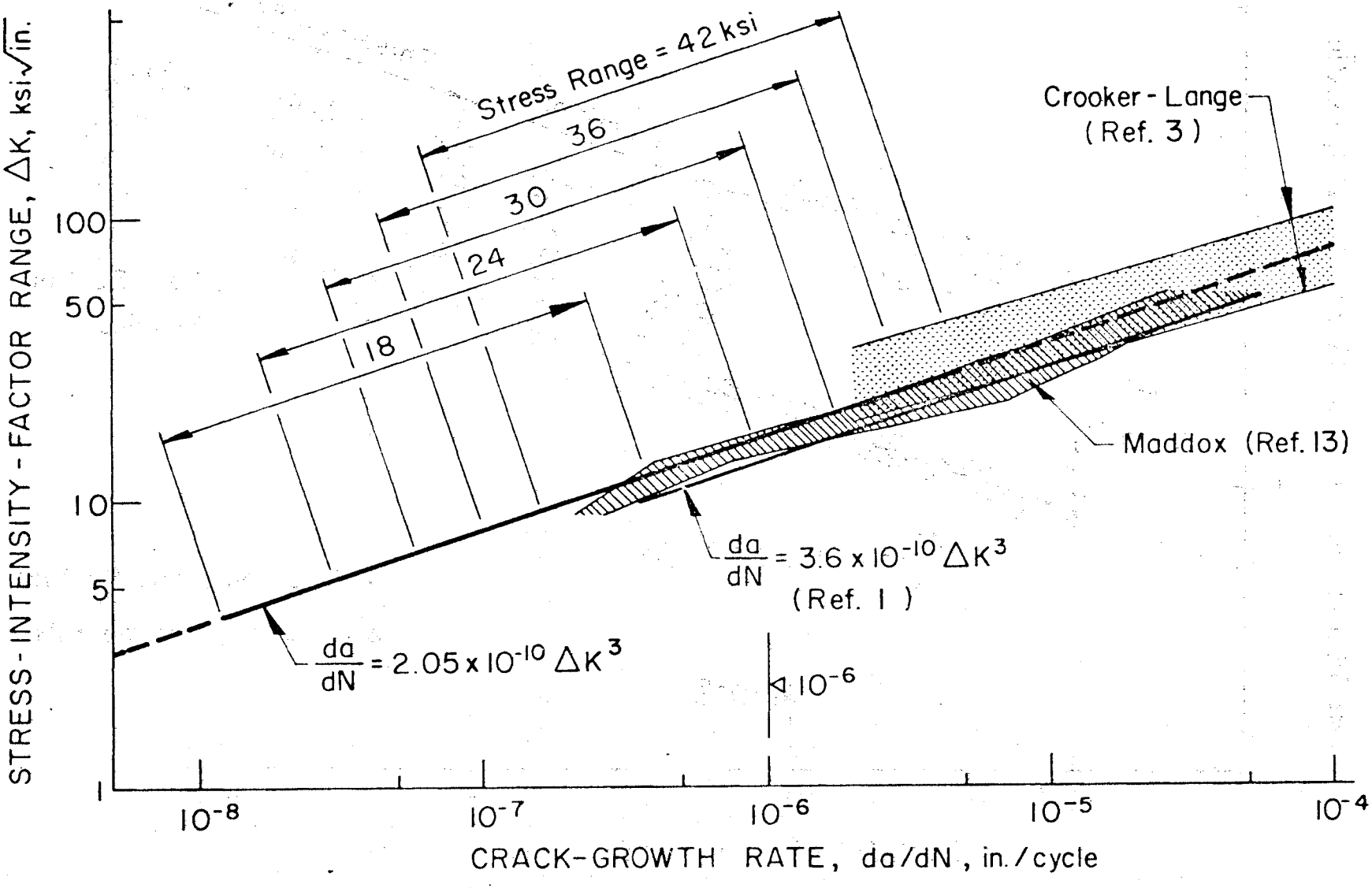

Fig. 9 Ranges for crack growth as a penny-shaped crack. Scatterbands and an upper bound estimate from other crack growth studies.

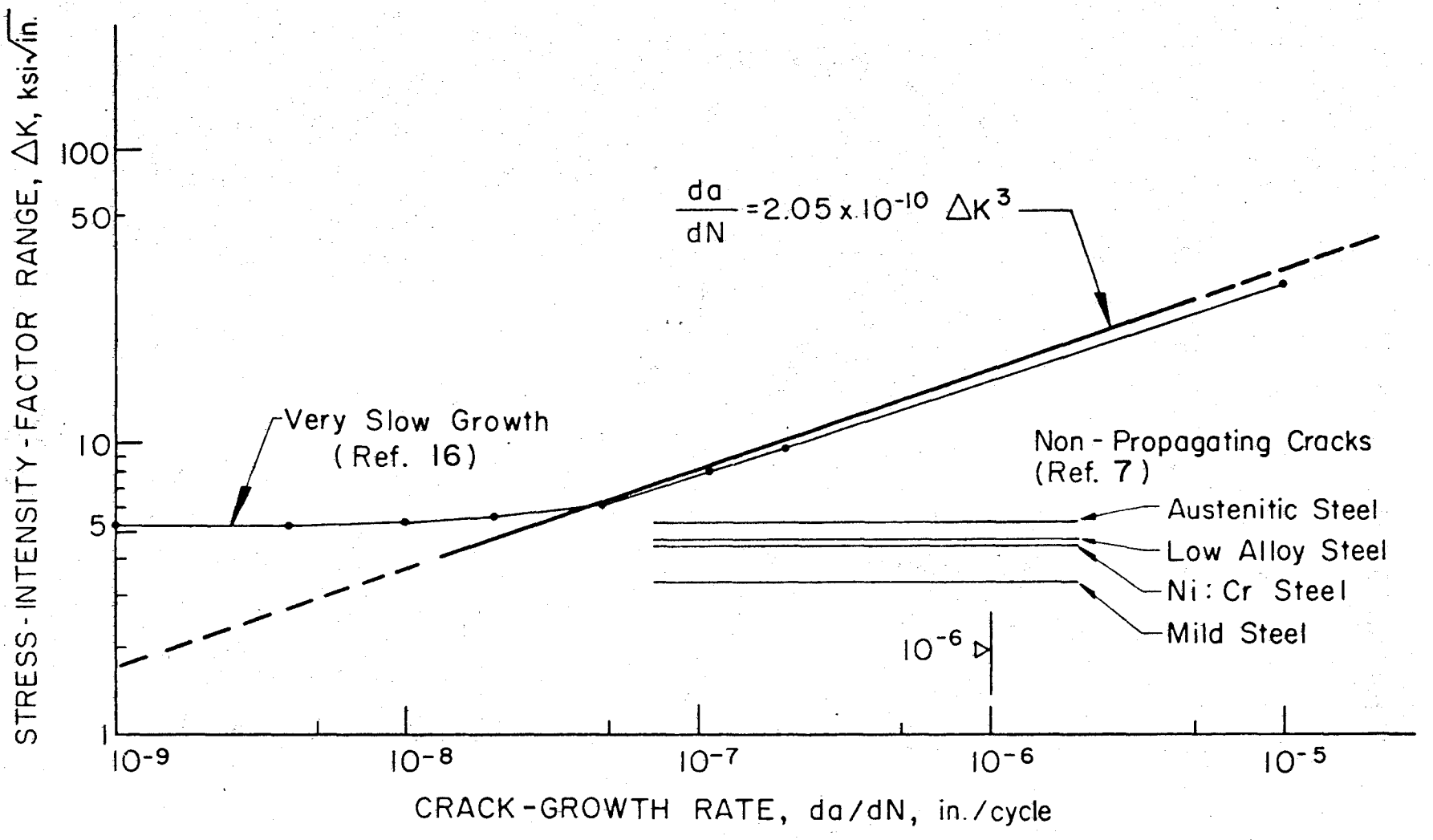

Fig. 10 Approximate mean line of Paris' data for very slow growth, and Harrison's limiting ΔK-values for non-propagating cracks

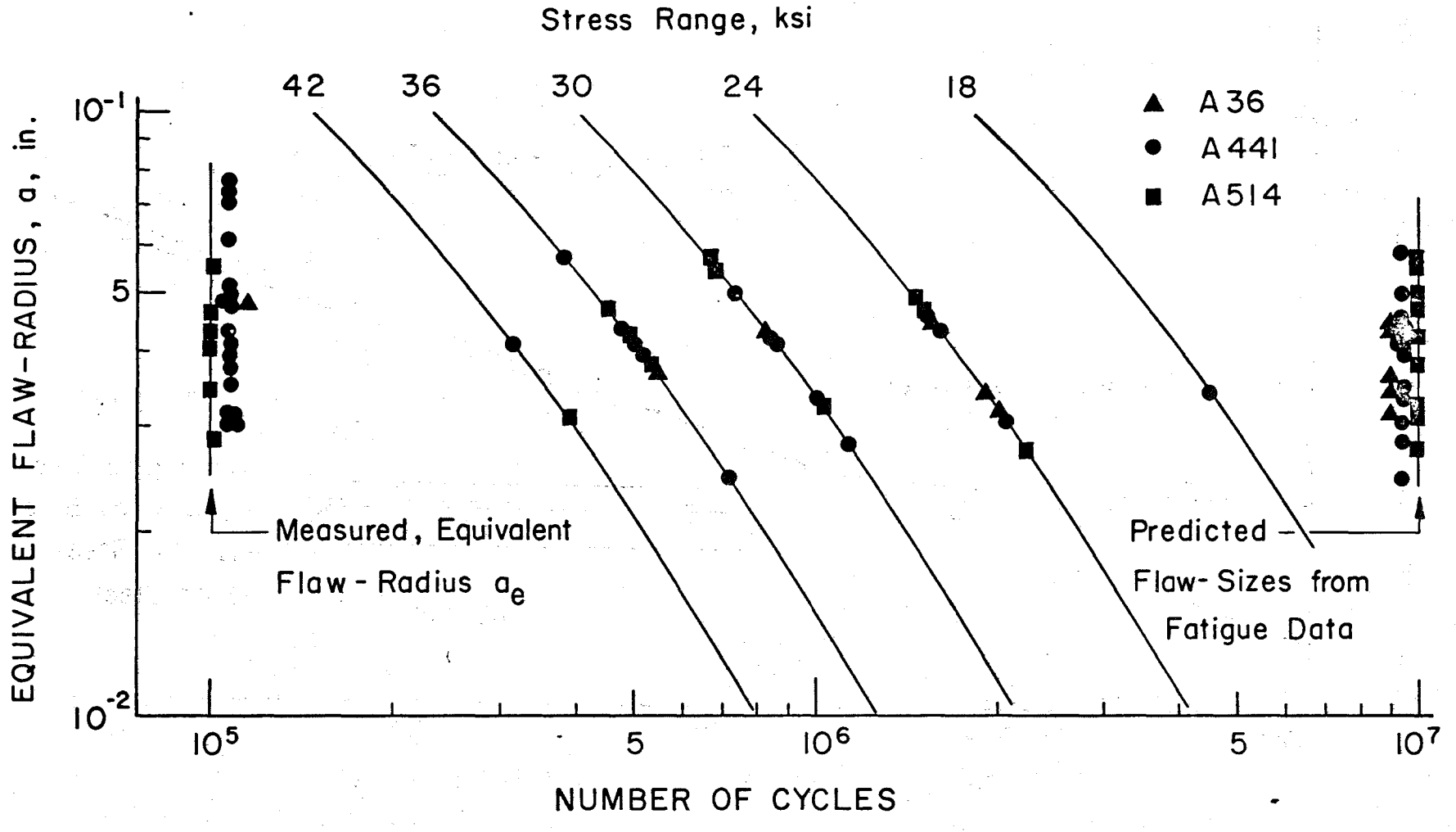

Fig. 11 Comparison of the scatter of measured equivalent flaw-sizes with the scatter of flaw-sizes derived from fatigue data

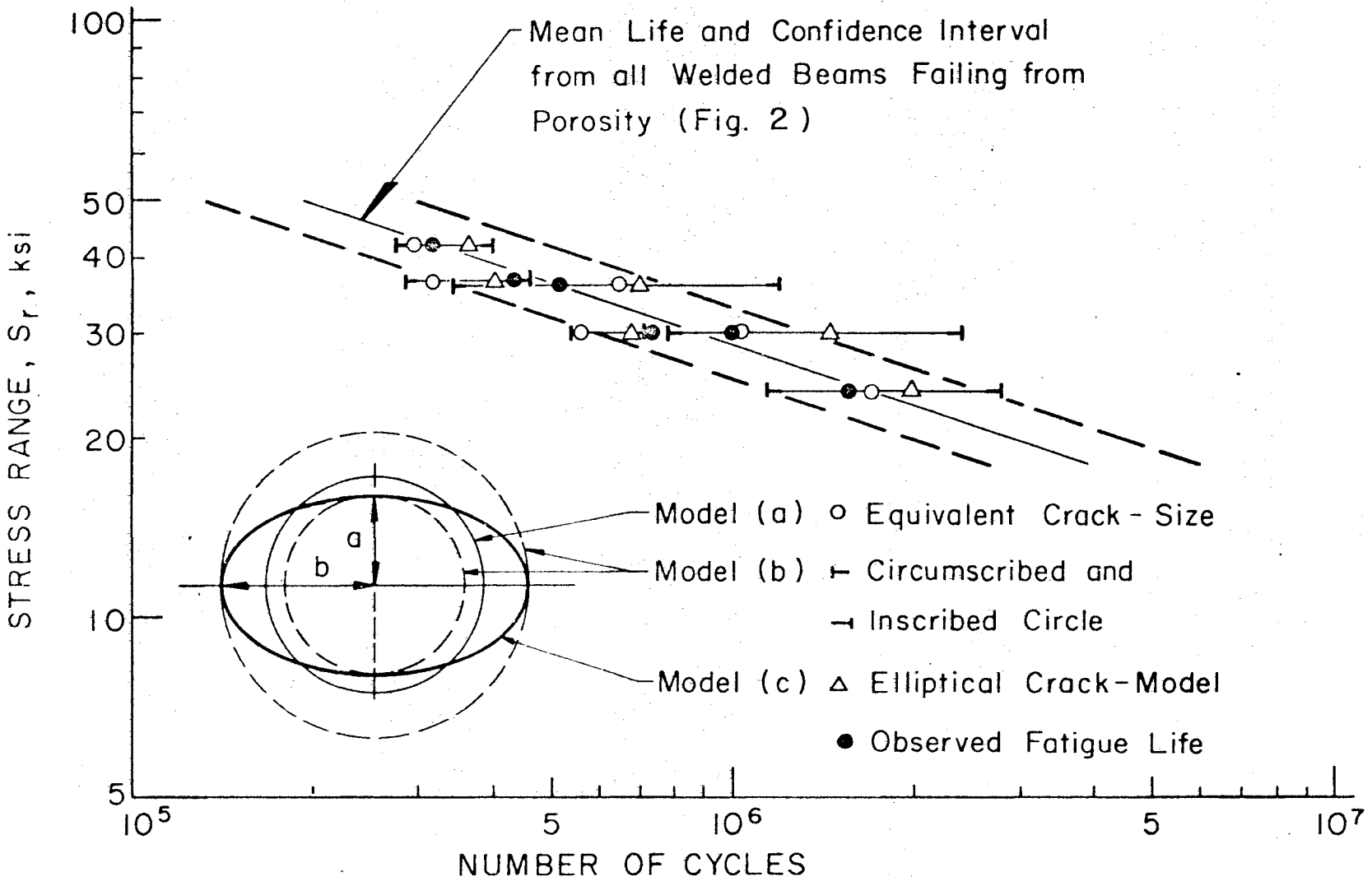

Fig. 12 Prediction of fatigue life using various crack-models

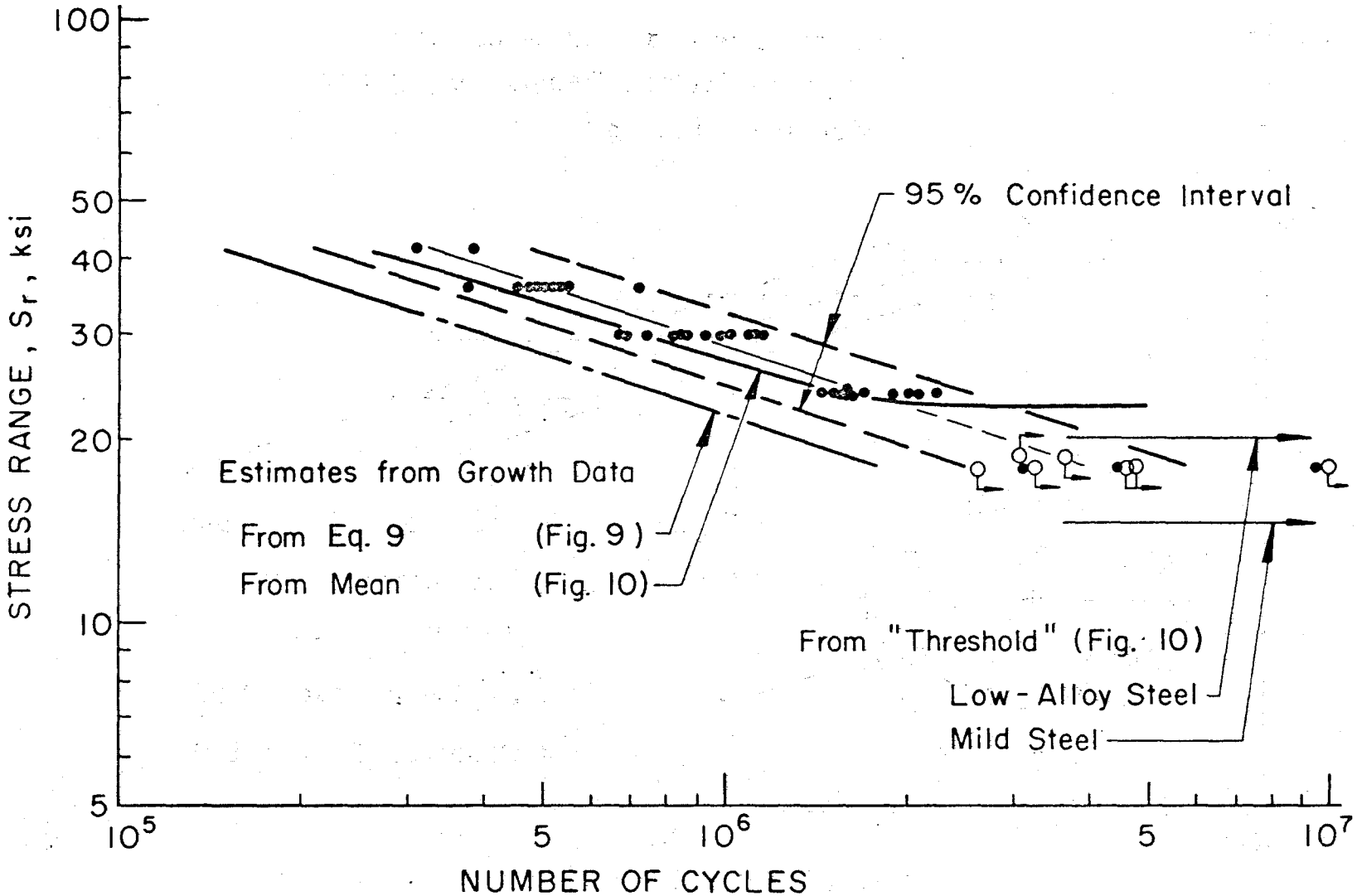

Fig. 13 Comparison of a predicted lower bound and a mean line with mean life and scatterband from test data

DOCUMENT CONTROL DATA - R & D

Security classification of title, body of abstract and indexing annotation must be entered when the overall report is classified)

1. ORIGINATING ACTIVITY (Corporate author) Lehigh University	2a. REPORT SECURITY CLASSIFICATION Unclassified 2b. GROUP

3. REPORT TITLE
FATIGUE CRACK GROWTH IN WELDED BEAMS

4. DESCRIPTIVE NOTES (Type of report and inclusive dates)

5. AUTHOR(S) (First name, middle initial, last name)
M. A. Hirt, J. W. Fisher

6. REPORT DATE January 1972	7a. TOTAL NO. OF PAGES 40	7b. NO. OF REFS 16
8a. CONTRACT OR GRANT NO. N00014-68-A-0514 b. PROJECT NO. 358 c. d.	9a. ORIGINATOR'S REPORT NUMBER(S) Fritz Eng. Lab. Rep. No. 358.35 9b. OTHER REPORT NO(S) (Any other numbers that may be assigned this report)	

10. DISTRIBUTION STATEMENT
"Approved for public release; Distribution unlimited".

11. SUPPLEMENTARY NOTES	12. SPONSORING MILITARY ACTIVITY Office of Naval Research

13. ABSTRACT

The fatigue behavior of welded steel beams is evaluated using the fracture mechanics concepts of stable crack growth. A fracture mechanics model for cracks originating from the pores in the web-to-flange fillet weld is developed. Estimates of the stress-intensity factor are made that numerically describe the initial flaw condition. With the final crack size known, a theoretical crack-growth equation was derived from the fatigue test data of the welded beams. The derived relationship compares well with actual crack-growth measurements on a welded beam and available data from crack growth specimens. The regime of crack growth where most of the time is spent growing a fatigue crack in a structural element is shown to correspond to growth rates below 10^{-6} in. per cycle. Little experimental crack growth data is available at this level. It is concluded that the fracture mechanics concepts can be used to analyze fatigue behavior and to rationally evaluate the major variables that influence the fatigue life of welded beams.

14 KEY WORDS	LINK A		LINK B		LINK C	
	ROLE	WT	ROLE	WT	ROLE	WT